Molecular structure and electronic properties of the quasi-one-dimensional discotic liquid crystal conductors hexakis (*n*-alkoxy) triphenylene

P. Etchegoin*
Centro Atómico Bariloche y Instituto Balseiro, Comisión Nacional de Energía Atómica y Universidad Nacional de Cuyo, 8400-San Carlos de Bariloche, Río Negro, Argentina
(Received 14 January 1997)

Quantum chemical calculations by means of the semiempirical *modified neglect of diatomic overlap* and *Austin model 1* (AM1) methods are presented for hexakis (*n*-alkoxy) triphenylene with $n=1$ and 4. The predicted molecular structures by the self-consistent electronic field are presented and discussed. The optimized geometries are then used to study the interaction between two molecules and the possible origin of the different experimentally observed conducting properties. In addition, the effect of dynamic and static disorder in the transport properties is briefly discussed in terms of the calculated electronic properties. Finally, a few basic aspects of the electron-doping process with $AlCl_3$ are bestowed. [S1063-651X(97)11406-4]

PACS number(s): 61.30.Cz, 31.15.Ct, 61.25.Em

I. INTRODUCTION AND OVERVIEW

The possibility of creating one-dimensional electronic conductors by means of weakly interacting molecules has been realized in discotic liquid crystals in recent years [1–5]. The basic idea is to produce hoppinglike transport by utilizing the considerable overlap among the *p* orbitals of neighboring aromatic rings, which normally form the core of discotic liquid crystal molecules. Hexakis (*n*-alkoxy)triphenylene (hereafter HAT*n*) is the prototype discotic liquid crystal with a disk-shaped molecular structure schematically shown in Fig. 1. In the columnar mesophases [6], discotic liquid crystals behave like one-dimensional fluids outlined by disordered stacks of disk-shaped molecules. The columnar mesophases have face-to-face molecules like that in Fig. 1, with typical separations among them in the range between 3 and 4 Å. As a result, a noteworthy overlap of *p* orbitals in the aromatic rings is expected. This overlap of orbitals produces a repulsive interaction [7] and favors certain orientations of one molecule with respect to another, as we shall show later. In addition, it provides a hoping mechanism for carriers along the stack of molecules. When observing the intrinsic transport properties in the columnar mesophases of HAT*n*, however, the large band gap in these quasi-one-dimensional conductors ($\sim$ 7 eV according to our calculation) and the low intrinsic carrier densities combine to make them insulators. The real breakthrough came with the work of Boden *et al.* [1,9] which provided the awareness that these triphenylenes can be conveniently doped by using electron acceptors like $AlCl_3$ or $NOBF_4$ in a process akin to that found in doped semiconductors. In this manner, a radical cation is formed by extracting an electron from the central backbone of aromatic rings in Fig. 1 [5,10] and hole conduction is established. The actual value of the carrier concentration is governed by the amount of doping and dc-conductivities of the order of $\sigma_{\parallel}\sim 10^{-4}\Omega^{-1}$ cm^{-1} can be obtained and have been measured for transport along the columns [11] in both the crystalline (K, $T=320$ K) and liquid crystalline (D_{ho}, $T=368$ K) phases.

The realization of charge-carrier transport in liquid crystal based conductors has opened important new possibilities. Essentially, conventional polymeric photoconductors for technological applications have a big impediment in their low intrinsic mobilities. The use of conjugated polymers [12] partly solves this problem but liquid crystal based photoconductors have also been proposed as serious candidates. Moreover, these materials can be easily oriented *in situ* by means of external magnetic or electric fields, making them suitable in situations where polymer-based conductors have hitherto not worked. These possibilities have been explored by different authors, notably the group of Haarer and coworkers [13–15]

Notwithstanding the significant importance of these materials as organic conductors with novel properties, there is no previous detailed study of the electronic structure of HAT*n* molecules to the best of our knowledge. The situation is in

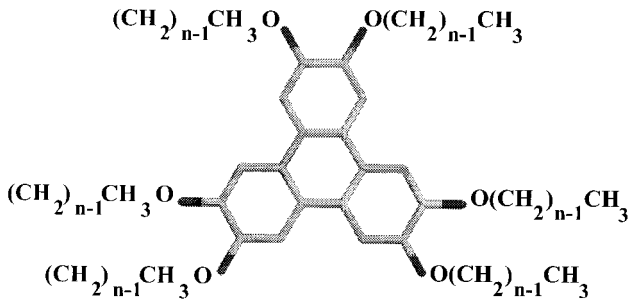

FIG. 1. Schematic basic structure of hexakis (*n*-alkoxy)triphenylene. The central core of aromatic rings is linked to six $O(CH_2)_{(n-1)}CH_3$ branches with variable length depending on *n*. Roughly speaking, electron delocalization in the central ring structure takes place and these *p* electrons can overlap with adjacent molecules providing a mechanism for hopping conduction upon doping. The side branches of the rings do not participate directly in the hybridization mechanism but their presence (and length) is important to establish the actual liquid crystalline properties of the different mesophases with variable *n*.

*Electronic address: etchegoi@cab.cnea.edu.ar

fact more general than that and the same can be said for other conducting liquid crystalline metal complexes such as the phthalocyanine [16]. The bulk of the work is concentrated in experimental determinations of conductivities as a function of frequency and temperature [5] for different orientations with respect to the columnar structure, as well as transient photoconductivity [13–15] experiments using time of flight techniques. The analysis of the experimental data is somewhat based on (correct) presumptions of how the electrons behave in these molecules but no detailed calculation of the wave functions, interactions among molecules, doping process, bandwidths for conduction along the columns, etc., exist in the literature. This work is a small contribution to fill that gap. A calculation of the electronic structure of two members of the family HATn ($n=1$ and 4) is presented. The reason for selecting these two particular molecules will be clear afterward; suffice it to say now that these two molecules account for the clear separation and the different roles of the electrons in the aromatic rings and the $(CH_2)_{(n-1)}CH_3$ branches (see Fig. 1).

By definition, the complete information of the calculation is contained in the full set of atom coordinates, wave functions, and eigenvectors. Still, this a formidable amount of data, which makes unintelligible the essential information needed to understand the basic physical phenomena observed experimentally. The latter depends mostly on the properties of the ground state wave function and a finite number of parameters like the total energy or hopping probability of carriers. For that reason, the only systematic data provided in tabular form are the optimized geometries of the molecules (as given by the self-consistent electronic field) and total, core-core, and electronic energies. The ground state wave function is given in a simplified form utilizing the advantage that it uses only one p orbital per carbon in the aromatic rings. The interaction between two HAT1 molecules is subsequently studied as well as the doping process with $AlCl_3$. The essential details of the ground state wave functions and charge distributions are discussed, placing emphasis on the physical consequences of the predicted electronic properties rather than on the accretion of numerical data.

The paper is organized as follows: Sec. II gives a brief description of the method, motivation and input data for the calculations. Section III presents the results and a brief description of their main consequences. Section IV is a short outline of future perspectives and open questions.

II. THE METHOD

In order to obtain the optimized geometries of the molecules and their electronic properties we use the Austin model 1 [17] (AM1) as well as the modified neglect of diatomic overlap (MNDO) methods [18] for comparison. In fact, the AM1 quantum mechanical molecular model was an improvement over the MNDO method. The MNDO Hamiltonian had several shortcomings in reproducing hydrogen bonds, which were overcome by AM1 [17,18]. Additional terms such as the one-center Coulomb and exchange integrals have been treated in AM1 as adjustable parameters with respect to MNDO, pushing the limits of the method through a prudently extended parametrization. All values in the discussion correspond to results by means of the AM1 Hamiltonian unless stated otherwise. Being semiempirical in essence, both methods have an impressive record of predictions in molecules containing both organic and inorganic subunits. The basic approximations and parameters of the methods as well as several results for hundreds of molecules and some polymers obtained with them have been extensively documented in the literature [17–20] and, accordingly, we do not dwell on their explanation [21]. A historical account of their development up to the MNDO method (prior to AM1) has even been published by their creator [22].

The AM1 quantum mechanical model has several advantages at a minimum computational cost with respect to *ab initio* methods, principally in the geometry optimization stages of an unknown molecule. Semiempirical methods of this kind undoubtedly complement *ab initio* ones and allow quantum mechanical calculations to be outspread to situations that would otherwise be far beyond their reach. AM1 ranks among the best semiempirical methods available to date and has been widely used in quantum chemical problems including geometry optimizations, reaction dynamics, and thermochemistry [23]. For an updated review of the present status of these models, recent applications on fullerene chemistry and other problems, as well as performance comparisons among *ab initio*, density functional, and semiempirical methods, see the recent review article by Thiel [24].

Carbon and oxygen are represented in the AM1 and MNDO Hamiltonians by 4 orbitals (sp^3 hybridization) while hydrogen has only one s. The parametrization for the orbitals is taken from Ref. [17] for AM1 and Ref. [18] for MNDO. In this manner, the Hamiltonians are of size 144×144 for HAT1 and 252×252 for HAT4 according to the total number of atoms. The calculation is performed with the integrated molecular package (MOPAC) version 6 developed by Stewart and Dewar [25]. The geometry optimization is performed by minimizing the self-consistent electronic field of the ground state as a function of a multidimensional displacement vector $\vec{r}=[r_i]$, to obtain the minimum total energy. The displacement vector represents all the movements of the different atoms in the molecule compatible with symmetry restrictions. In fact, symmetry operations can be conveniently used to minimize the dimension of the hyperspace where the minimum must be found. The starting input geometry has to be inferred from similar structures in other organic molecules. The trial values for the geometry of the central aromatic rings in Fig. 1 were taken from the available structural data on benzene [26] for both HAT1 and HAT4. In the case of HAT1, the six OCH_3 branches affixed to the central core of aromatic rings have the basic structure of the methoxyl radical and their tentative geometry was obtained from the available data in the literature [27] for this compound. On the other hand, the six C_4H_9 branches in HAT4 have the basic structure of a polyethylene segment except, of course, for the CH_3 endings and the first bond to the oxygen. Typical structural parameters for *trans* polyethylene [28] were used for these branches as trial coordinates in the search for a self-consistent electronic field (SCF). Finally, the electronic structure of $AlCl_3$ has also been calculated to evaluate its electron affinity and study the doping process of the liquid crystals. The trial structural parameters of the latter

TABLE I. Optimized geometry from the self-consistent electronic field of the AM1 Hamiltonian for HAT1. (1) Central carbons in the aromatic rings; (2) hydrogens of the aromatic rings; (3) oxygen links with the CH_3 branches; (4) = carbons in the CH_3 branches; (5) hydrogens in the CH_3 branches.

Atom type	x (Å)	y (Å)	z (Å)
C^1	0.0000	0.0000	0.0000
C^1	1.4335	0.0000	0.0000
C^1	2.1282	1.2033	0.0000
C^1	1.4211	2.4281	0.0000
C^1	2.1473	3.6860	0.0000
C^1	3.5616	3.6860	0.0000
C^1	4.2564	4.8894	0.0000
C^1	3.5396	6.1308	0.0000
C^1	2.1501	6.1308	0.0000
C^1	1.4430	4.9060	0.0000
C^1	−0.0095	4.9060	0.0000
C^1	−0.7167	6.1308	0.0000
C^1	−2.1061	6.1308	0.0000
C^1	−2.8229	4.8894	0.0000
C^1	−2.1281	3.6860	0.0000
C^1	−0.7138	3.6860	0.0000
C^1	0.0124	2.4281	0.0000
C^1	−0.6947	1.2033	0.0000
H^2	3.2239	1.1613	0.0000
H^2	4.1458	2.7581	0.0000
H^2	1.6387	7.1007	0.0000
H^2	−0.2052	7.1007	0.0000
H^2	−2.7123	2.7581	0.0000
H^2	−1.7904	1.1613	0.0000
O^3	−0.6572	−1.1547	0.0000
O^3	2.0906	−1.1547	0.0000
O^3	5.5850	4.8976	0.0000
O^3	4.2111	7.2773	0.0000
O^3	−2.7776	7.2773	0.0000
O^3	−4.1515	4.8976	0.0000
C^4	−1.3411	−2.3565	0.0000
C^4	2.7746	−2.3565	0.0000
C^4	6.9677	4.9062	0.0000
C^4	4.9099	8.4705	0.0000
C^4	−3.4764	8.4705	0.0000
C^4	−5.5342	4.9062	0.0000
H^5	−1.9779	−2.3868	0.9235
H^5	−1.9705	−2.3911	−0.9285
H^5	−0.5808	−3.1819	0.0049
H^5	3.4114	−2.3868	−0.9235
H^5	3.4039	−2.3911	0.9285
H^5	2.0143	−3.1819	−0.0049
H^5	7.3124	4.3699	0.9235
H^5	7.3123	4.3784	−0.9285
H^5	7.3024	5.9773	0.0049
H^5	4.6177	9.0371	−0.9235
H^5	4.6251	9.0328	0.9285
H^5	6.0048	8.2248	−0.0049
H^5	−3.1843	9.0371	0.9235
H^5	−3.1916	9.0328	−0.9285
H^5	−4.5713	8.2248	0.0049
H^5	−5.8789	4.3699	−0.9235
H^5	−5.8788	4.3784	0.9285
H^5	−5.8689	5.9773	−0.0049

have been taken from Ref. [29] assuming D_{3h} (planar) symmetry.

III. RESULTS AND DISCUSSION

A. Structural parameters

We present here the optimized geometries obtained from the SCF Hartree-Fock electronic field using the AM1 Hamiltonian. The geometry of a given molecule can always be supplied in terms of internal coordinates by providing, for each atom, a reference distance to a second one, a reference angle to a third, and a dihedral angle using a fourth. Even though most quantum chemical calculations are most frequently put in terms of internal coordinates (including this), we prefer for presentation purposes simple Cartesian coordinates to provide the optimized geometries. In this manner, we use the intrinsic simplicity imposed by the planar central structure of the molecule and we avoid three additional columns with the reference atoms in each table. The symmetry restrictions imposed on each molecule to find the total energy minimum are simple; atoms that are symmetry equivalent are restricted to move in the same manner relative to their neighbors. Both HAT1 and HAT4 have an overall D_{3h} symmetry in their molecular structures. Tables I and II show the optimized geometries in Cartesian coordinates for HAT1 and HAT4, respectively. Note that the only out-of-plane atoms in both structures are the hydrogens of the $(CH_2)_{(n-1)}CH_3$ branches; the molecule is planar otherwise. The values in Table I and II are mainly given for future reference, plotting purposes by other authors and, eventually, direct comparison with *ab initio* methods or x-ray data. Schematic views of the structures represented by the data in Tables I and II in both ball-and-stick and spacefill forms are given in Figs. 2 and 3. Once the SCF has been achieved and the molecular structures calculated with AM1, we proceed with the description of the principal electronic properties.

B. Electronic properties

Table III shows the most important macroscopic electronic properties of both molecules calculated with the AM1 and MNDO Hamiltonians, respectively. The total energy of each molecule is the sum of the total (positive) core-core repulsions of the bare atomic cores without the valence electrons plus the total (negative) electronic energies. The ionization potential is equal to minus the energy of the highest occupied molecular orbital level, according to Koopman's theorem [21]. The values in Table III convey a general sense of the changes introduced by the improved parametrization of AM1 with respect to MNDO. Note that total electronic and core-core energies are within 1% of each other for both methods. Differences occur, however, for the heats of formation, which are given relative to the elements in their standard state [30,31]. A more interesting picture is obtained by taking a closer look at the electronic structure and, in particular, at the ground-state wave functions and charge distributions. Before we move on with the latter, it is convenient to point out the reason for the selection of the two molecules HAT1 and HAT4. It is generaly accepted that the electronic structure of these molecules can be roughly separated into two parts. The aromatic rings have delocalized electrons in

TABLE II. Optimized geometry from the self-consistent electronic field of the AM1-Hamiltonian for HAT4. (1) Central carbons in the aromatic rings; (2) hydrogens of the aromatic rings; (3) oxygen links with the C_4H_9 branches; (4) carbons in the C_4H_9 branches; (5) hydrogens in the C_4H_9 branches.

Atom type	x (Å)	y (Å)	z (Å)	Atom type	x (Å)	y (Å)	z (Å)
C^1	0.0000	0.0000	0.0000	H^5	−1.0280	−2.9144	−0.9284
C^1	1.4329	0.0000	0.0000	H^5	−1.0214	−2.9183	0.9238
C^1	2.1279	1.2039	0.0000	H^5	−3.1181	−1.4999	0.9093
C^1	1.4209	2.4286	0.0000	H^5	−3.1251	−1.4989	−0.8946
C^1	2.1472	3.6866	0.0000	H^5	−3.3128	−4.0173	−0.8963
C^1	3.5613	3.6866	0.0000	H^5	−3.3061	−4.0176	0.9102
C^1	4.2564	4.8905	0.0000	H^5	−5.4063	−2.6274	−0.8956
C^1	3.5400	6.1314	0.0000	H^5	−5.6320	−4.1687	0.0292
C^1	2.1498	6.1314	0.0000	H^5	−5.3923	−2.6055	0.9147
C^1	1.4427	4.9067	0.0000	H^5	2.4610	−2.9144	0.9285
C^1	−0.0099	4.9067	0.0000	H^5	2.4543	−2.9183	−0.9238
C^1	−0.7170	6.1314	0.0000	H^5	4.5510	−1.4999	−0.9093
C^1	−2.1071	6.1314	0.0000	H^5	4.5579	−1.4989	0.8946
C^1	−2.8235	4.8905	0.0000	H^5	4.7457	−4.0173	0.8963
C^1	−2.1285	3.6866	0.0000	H^5	4.7208	−4.0281	−0.8970
C^1	−0.7143	3.6866	0.0000	H^5	6.8392	−2.6274	0.8956
C^1	0.0120	2.4286	0.0000	H^5	7.0649	−4.1687	−0.0292
C^1	−0.6951	1.2039	0.0000	H^5	6.8252	−2.6055	−0.9147
H^2	3.2234	1.1613	0.0000	H^5	7.2944	5.4574	−0.9285
H^2	4.1460	2.7592	0.0000	H^5	7.2944	5.4652	0.9237
H^2	1.6390	7.1015	0.0000	H^5	7.1143	2.9401	0.9093
H^2	−0.2061	7.1015	0.0000	H^5	7.1171	2.9336	−0.8947
H^2	−2.7132	2.7592	0.0000	H^5	9.3919	4.0302	−0.8963
H^2	−1.7906	1.1613	0.0000	H^5	9.3888	4.0362	0.9102
O^3	−0.6586	−1.1548	0.0000	H^5	9.2350	1.5222	−0.8956
O^3	2.0915	−1.1548	0.0000	H^5	10.6827	2.0974	0.0292
O^3	5.5858	4.8976	0.0000	H^5	9.2090	1.5234	0.9147
O^3	4.2108	7.2792	0.0000	H^5	5.5500	8.4789	0.9284
O^3	−2.7779	7.2792	0.0000	H^5	5.5566	8.4751	−0.9238
O^3	−4.1530	4.8976	0.0000	H^5	3.2800	9.5818	−0.9094
C^4	−1.3475	−2.3628	0.0000	H^5	3.2754	9.5872	0.8945
C^4	2.7804	−2.3628	0.0000	H^5	5.3628	11.0090	0.8962
C^4	6.9764	4.9050	0.0000	H^5	5.3662	11.0034	−0.9103
C^4	4.9125	8.4798	0.0000	H^5	3.1122	12.1272	0.8956
C^4	−3.4796	8.4798	0.0000	H^5	4.3342	13.0933	−0.0292
C^4	−5.5435	4.9050	0.0000	H^5	3.1003	12.1041	−0.9147
C^4	−2.8462	−2.1052	0.0060	H^5	−4.1170	8.4789	−0.9284
C^4	−3.5996	−3.4177	0.0082	H^5	−4.1237	8.4751	0.9238
C^4	−5.0896	−3.1926	0.0142	H^5	−1.8470	9.5817	0.9093
C^4	4.2791	−2.1052	−0.0060	H^5	−1.8427	9.5873	−0.8946
C^4	5.0324	−3.4177	−0.0082	H^5	−3.9298	11.0091	−0.8963
C^4	6.5225	−3.1926	−0.0142	H^5	−3.9334	11.0034	0.9103
C^4	7.5027	3.4782	0.0060	H^5	−1.6794	12.1272	−0.8956
C^4	9.0160	3.4820	0.0082	H^5	−2.9013	13.0933	0.0292
C^4	9.5661	2.0791	0.0142	H^5	−1.6674	12.1041	0.9147
C^4	3.9400	9.6489	−0.0060	H^5	−5.8615	5.4575	0.9284
C^4	4.7000	10.9576	−0.0082	H^5	−5.8615	5.4652	−0.9238
C^4	3.7601	12.1355	−0.0142	H^5	−5.6817	2.9402	−0.9094
C^4	−2.5071	9.6489	0.0060	H^5	−5.6840	2.9336	0.8945
C^4	−3.2671	10.9576	0.0082	H^5	−7.9591	4.0303	0.8962
C^4	−2.3272	12.1355	0.0142	H^5	−7.9559	4.0361	−0.9103
C^4	−6.0698	3.4782	−0.0060	H^5	−7.8021	1.5222	0.8956
C^4	−7.5831	3.4820	−0.0082	H^5	−9.2498	2.0974	−0.0292
C^4	−8.1333	2.0791	−0.0142	H^5	−7.7761	1.5234	−0.9147

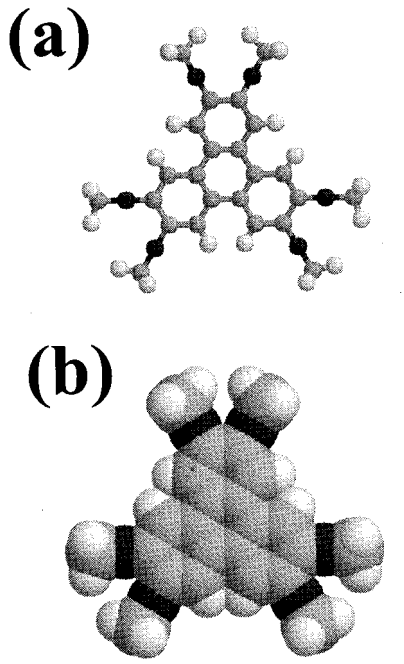

FIG. 2. Schematic view of the optimized geometry of HAT1 from the electronic structure by means of the AM1 Hamiltonian: (a) ball-and-stick and (b) space fill representations. In both cases the atoms are: carbon→grey, hydrogen→light-grey, and oxygen →black. Note the the hydrogens in the CH_3 endings affixed to the oxygens are the only out-of-plane atoms. See Table I for the full Cartesian coordinates of this structure.

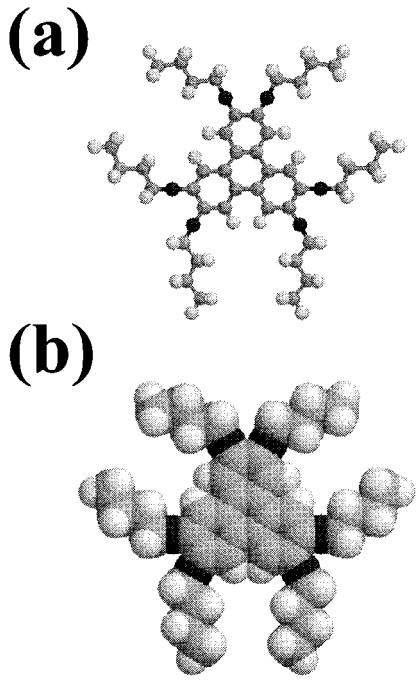

FIG. 3. Same as Fig. 2 but for HAT4. The only out-of-plane atoms in this structure are the hydrogens of the C_4H_9 *polyethylene-like* branches. See text for further details and Table II for the full list of Cartesian coordinates of this molecular structure.

the p_z orbitals of carbon that form the ground state. The oxygen links serve as a sort of barrier between the electronic structure of the central rings and the $(CH_2)_{(n-1)}CH_3$ branches in the ground state. The optical properties in the transparency region [32] and the hybridization process in the columnar mesophases are therefore directly related to the electronic properties of the central core of rings. On the other hand, the length and characteristics of the $(CH_2)_{(n-1)}CH_3$-side chains are of prime importance in the determination of the specific liquid crystalline properties and can change transition temperatures to the different mesophases and the overall physical picture. A similar phenomenon is well known in nematic liquid crystal homologs and is related to the effect of the side chains on them. To be more specific, let us take the example of the cyano-biphenyl homologs 4-cyano-4-*n*-alkylbiphenyls, best known as *n*-CB. These molecules constitute a clear example of how different parts of the molecule with relatively isolated electronic structures contribute to distinct physical properties of the mesophases. The cyano terminal group attached to the phenyl rings is the principal contributor to the dielectric anisotropy of the molecule [33] while the flexibility and, principally, the length of the alkyl side chain ($C_nH_{(2n-1)}$) changes the type of mesogenic phases and their critical temperatures. Short side chains are associated with the absence of liquid crystalline phases or low transition temperatures to the nematic state (e.g., 2CB and 4CB). Longer side chains show nematic phases with increasing critical temperatures and the eventual appearance of the smectic-*A* (S_A) phase. The goal in HAT*n* is therefore to show the different roles played by the central electrons in the phenyl rings with respect to the side branches. We shall show that the electronic structure of the core is essentially unchanged when increasing the length of the $(CH_2)_{(n-1)}CH_3$-side chains and that the ground state wave functions of the two molecules are basically the same and principally localized in the p_z orbitals of the central rings.

Table IV summarizes the calculated charge, electron density, and ground state wave function coefficients of HAT1 and HAT4 on the different atoms of the structure. In order to reduce the amount of information we use the following properties of HAT*n* valid for the ground state: (i) there are only three different types of carbons in the central rings for both HAT1 and HAT4; the others are symmetry related to these three and they appear as C1, C2, and C3 in Fig. 4; (ii) the oxygens (O in Fig. 4) are symmetry related and therefore it is sufficient it to specify the ground state electronic properties for one; (iii) the side hydrogens in the central rings (H1 in Fig. 4) are also symmetry equivalent; (iv) the ground state wave function has negligible projection over the carbons and hydrogens of the side chains and we provide, accordingly, representative values for them without distinguishing the different positions along the chain; we represent them by a generic Cn and Hn in both Fig. 4 and Table IV; (v) the ground state wave function comprises only p_z orbitals of C1, C2, C3, and O and therefore, a massive simplification occurs in the coefficients of the wave function given in Table IV. The electron density on each atom is the number of valence electrons on it while the charge is defined as the sum of the (negative) electron density and the positive core charge [25]. Table IV shows clearly that the ground state wave function, which is completely localized in the central rings and the oxygen links, is perturbed very little on going from HAT1 to HAT4. We therefore conclude that there is a clear separation

TABLE III. Calculated basic electronic properties with the MNDO and AM1 Hamiltonians for HAT1 and HAT4. The molecules have molecular weigths of 408.45 and 660.932 a.u. of mass, respectively.

AM1 Hamiltonian	HAT1	HAT4
Total energy (eV)	−5309.98	−8114.99
Electronic energy (eV)	−41641.37	−88033.38
Core-core repulsion (eV)	36331.38	79918.38
Ionization potential (eV)	7.127	6.979
Heat of formation (kcal)	167.64	44.64
MNDO Hamiltonian	**HAT1**	**HAT4**
Total energy (eV)	−5332.26	−8148.29
Electronic energy (eV)	−41453.31	−87229.86
Core-core repulsion (eV)	36121.04	79081.57
Ionization potential (eV)	7.425	7.330
Heat of formation (kcal)	6.43	−78.18

between the electronic properties of the central core and the side chains and that the former contributes primarily to the ground state electronic properties. We shall assume henceforth that this property holds for all the members of the HAT*n* family.

It is interesting to note, on the other hand, that the electronic density in the carbons of the side chains is comparable to that of the central rings. The charge distribution in both molecules is in fact fairly homogeneous in the triphenyls and the side chain carbons; the oxygens are the atoms with the highest electron density in both HAT1 and HAT4 (see Table IV). To illustrate this, we show in Fig. 4 a schematic ground state electron density map of HAT1 and HAT4 where we used the same scale for both molecules to make densities

TABLE IV. For the first column, see Fig. 4; The second column is the sum of the positive core charge plus negative of the number of valence electrons on the atom. The third column is number of valence electrons on the atom. The fourth column is squared coefficients in the ground state wavefunction on the given atom.

Atom	Charge	Elec. density	Ψ^2
	HAT1 ground state properties (AM1)		
C1	0.2762	3.7238	0.0494 (p_z)
C2	−0.2060	4.2060	0.02255 (p_z)
C3	−0.0162	4.0162	0.05795 (p_z)
O	−0.5771	6.5771	0.03193 (p_z)
H1	0.1463	0.8537	0.00000
Cn	0.2197	3.7803	< 0.0003
Hn*	0.050	0.946	< 0.0025
	HAT4 ground state properties (AM1)		
C1	0.2739	3.7261	0.0492 (p_z)
C2	−0.2088	4.2088	0.02250 (p_z)
C3	−0.0171	4.0171	0.05765 (p_z)
O	−0.5771	6.5771	0.03246 (p_z)
H1	0.1442	0.8558	0.00000
Cn	~ -0.22	~ 4.22	< 0.0003
Hn [a]	~ 0.08	~ 0.92	< 0.0025

[a]Average or representative values for the branches.

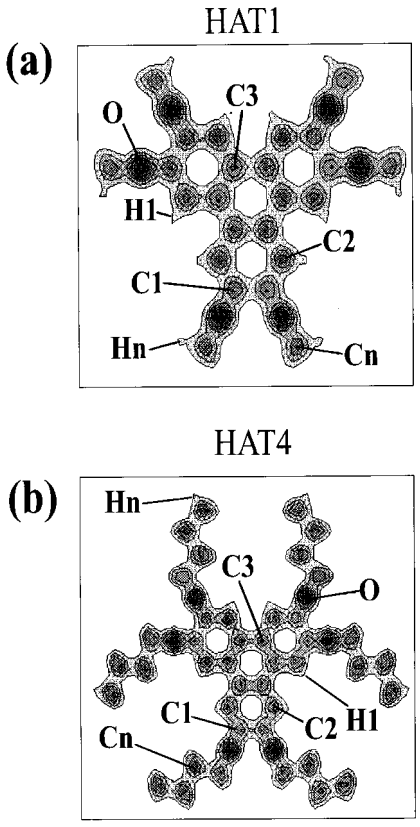

FIG. 4. Electron density map of HAT1 and HAT4. The sites labled as C1, C2, C3, O, H1, Cn, and Hn make reference to the atoms displayed in Table IV and form the minimun set of atoms needed to compare the ground state electronic properties of both molecules. The electronic density is schematically shown in this figure. Darker colors mean higher electron densities. We used the same scale for both molecules to make the comparison between the two possible. Note that this is a quasi-two-dimensional representation of the molecule where the out-of-plane hydrogens in the side chains are barely seen as small bumps around the carbons. The same holds for the in-plane hydrogens of the central rings. The electronic density is fairly constant throughout the molecule except at the oxygen positions. Both molecules have comparable charge distributions and the ground state wave funtion is in fact very little affected by the enlarged side chains of HAT4. See text for further details.

comparable. It is quite clear that, except for the oxygen links, the electron density distribution is fairly constant all over the molecules and similar for both.

The existence of more atoms in the side chains of HAT4 with respect to HAT1 results in the formation of additional molecular levels that are, roughly speaking, located below ~ -10 eV and around ~ 5 eV in the occupied and unoccupied electronic states, respectively. These are shown schematically in Fig. 5 and are part of the subject of the following subsection.

C. Two interacting HAT1 molecules

So far we have established that the electronic structure of the family of molecules HAT*n* can be separated into two distinct parts; the central rings and the side branches. The former determine the ground state wave function, which is

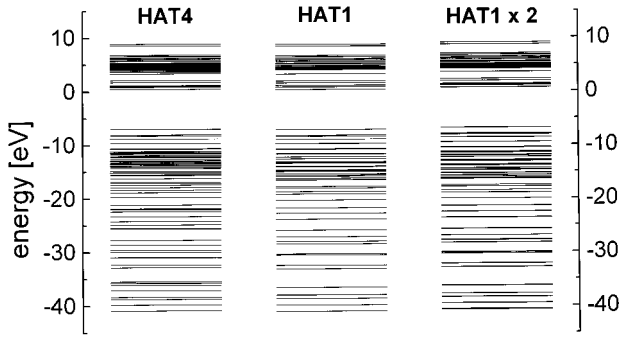

FIG. 5. Schematic energy level diagrams of HAT1, HAT4, and two interacting HAT1 (shown in Fig. 6). The inclusion of additional atoms in the side chains of HAT4 with respect to HAT1 results in a series of *valence* states below -10 eV and several unoccupied levels around 5 eV. The highest occupied and lowest unoccupied molecular levels are essentially the same for both molecules. The degeneracy of each state is not indicated. The energy levels of two interacting HAT1 is calculated at 4 Å separation between them and a twist angle of 60° as shown in Fig. 6. Further details are given in the text.

essentially built out of p_z orbitals of the central carbons and oxygens and are therefore perpendicular to the main plane of the molecule. It is instructive at this stage to look at the general energy level distribution of the two molecules for two reasons: firstly, to see how the above mentioned electronic properties echo in the level diagram and, secondly, to take in the proximity effect of a second molecule, which is the subject of this subsection.

Figure 5 schematically displays the energy level diagram of HAT1, HAT4, and two interacting HAT1 molecules, which we shall explain subsequently. The HAT1 molecule has 144 levels according to the number of orbitals being used in the AM1 Hamiltonian, 78 of which are *valence* states and are therefore populated. The highest occupied molecular orbital (HOMO) is fourfold degenerate and separated by a gap of 7.452 eV from the lowest unoccupied state (LUMO). The gap is given by the ionization potential (see Table III) plus the energy of the lowest unoccupied orbital (LUMO) with respect to vacuum and is not directly related to the optical absorption edge one would see in experiments [34]. On the other hand, HAT4 has 252 levels with 132 occupied valence states, a gap of 7.441 eV and the same fourfold degenerate ground state of HAT1 as shown in the previous section. By sorting the eigenvectors and eigenvalues and separating those introduced by the additional atoms in HAT4 we conclude that the *main* effect of increasing the length of the side chains is to create valence states below -10 eV and a dense unpopulated series of levels around 5 eV. The highest occupied and lowest unoccupied molecular levels are unaltered when going from HAT1 to HAT4.

Additionally, we would like to know further details of the interaction between two molecules to gain some insight into the band formation and carrier conduction. To this end, and taking into account the electronic properties that we have hitherto depicted, we shall study the interaction of two HAT1 molecules and assume they render the essential features of the full family of HAT*n* molecules. Working with two HAT1 molecules reduces considerably the computation time and the eigenvalue-eigenvector sorting of the calculation. Figure 5 shows the schematic level diagram of two interacting HAT1 molecules that should be compared to an isolated HAT1 molecule. However, in order to understand the origin of this level distribution it is indispensable to proceed with further details of the calculation and come back to Fig. 5 subsequently. The calculation is performed with two parallel HAT1 molecules facing each other with fixed structural parameters given by the AM1 Hamiltonian (see Table I and Fig. 2). The molecules are pushed along the line joining their centers and the self-consistent electronic field is optimized at each stage to obtain the core-core, electronic, and total energies. The molecules are allowed to rotate freely around their centers to find the minimum total energy but no other structural parameter is optimized otherwise.

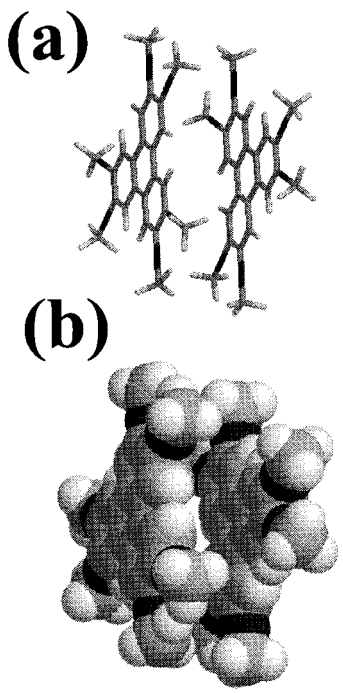

FIG. 6. Two interacting HAT1 molecules in sticks (a) and space fill representations (b). The structure of the individual molecules has been obtained from the AM1 geometry optimization given in Table I and are not reoptimized. The distance between the centers of the molecules is 4 Å and they are allowed to rotate in order to minimize the total energy. The overlap of p_z orbitals results in a rotation by 60° of one molecule with respect to the other. The band level diagram of the two interacting molecules for this separation distance is given in Fig. 5.

At large separation distances between the two molecules the total energy is obviously twice the total energy of a single one. On the other hand, as soon as the electronic clouds of the p_z orbitals start to weakly overlap, the molecules minimize the total energy by rotating. Figure 6 shows this situation schematically. The minimum total energy in their interaction corresponds to a 60° rotation of one molecule around its center with respect to the other. For this relative orientation of the molecules, shown in Fig. 6, we calculated the self-consistent electronic fields for different separation distances d. In Figs. 7 and 8 we show the core-core, electronic, and total energies, respectively. The interaction between two molecules is always repulsive [7] and there is a clear crossover in the total energy needed to push the

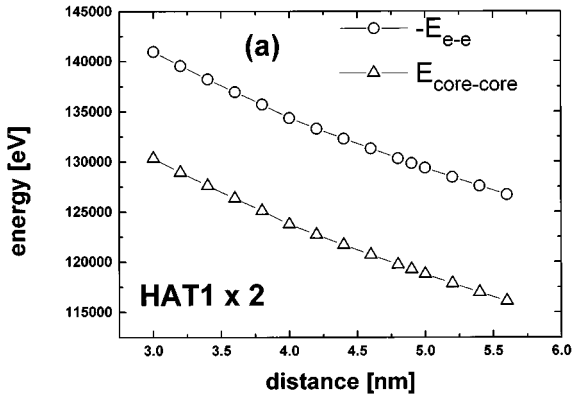

FIG. 7. Core-core repulsion ($E_{\text{core-core}}$) and electron energy ($E_{e\text{-}e}$) for the molecules shown in Fig. 6 as a function of their separation distance d. Note that the electronic energy is in fact negative and consequently the plot shows $-E_{e\text{-}e}$ in order to facilitate the vertical scale range. The difference between these two curves gives the total energy of the configurations which is displayed in Fig. 8.

molecules together around 4 Å according to Fig. 8. Obtaining the mean separation among molecules in the liquid or liquid crystalline state from the study of the microscopic interaction between two of them is normally impossible and stands as one of the most difficult questions of the liquid state. Among other things, it requires the knowledge of the thermodynamic *equation of state* or, equivalently, a detailed knowledge of the partition function including the interactions with the neighboring molecules in and outside a single column, a nontrivial task even for simple models of interactions in liquids. In liquid crystals, in addition, the mean field produced by the rest of the molecules is highly anisotropic in the ordered mesophases producing an even more difficult situation than in classical fluids. The latter is certainly beyond the aim of the present work. The most we can assert from the study of two interacting molecules is that the total energy increases sharply below certain limit when pushed face to face and this distance is presumably related or close to the minimum packing distance achievable in the D_{ho} and H columnar mesophases. We note incidentally that x-ray diffraction data in the parent compound 2,3,6,7,10,11-hexahexylthiotriphenylene [36,37] (HHTT), where oxygen is replaced by sulfur in the side chains, suggest an intracolumnar spacing (i.e., separation among molecules in a single column) of 3.64 Å . Note also that the rotation of one molecule with respect to another to minimize the total energy in their interaction is presumably related to the microscopic mechanism that brings forth the helical columnar (H) phase when the temperature is lowered from the D_{ho}. We shall come back to this problem later.

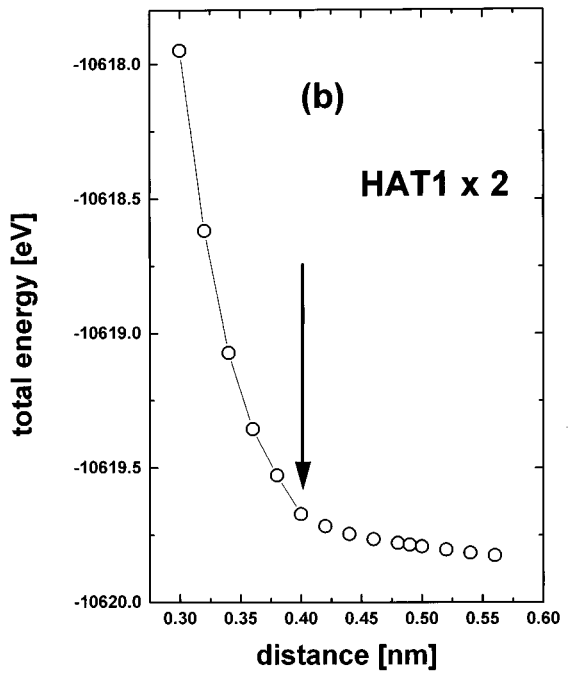

FIG. 8. Total energy of the molecules in Fig. 6 as a function of d. Notice the crossover around $\sim$ 4 Å in the total energy needed to push two molecules against each other. This is presumably the minimum packing intracolumnar distance in the D_h and H mesophases of this discotic liquid crystal. See text for further explanation.

By assuming a typical molecular separation of 4 Å we obtain the band energy diagram shown in Fig. 5 as HAT1 $\times 2$ for two molecules. The main consequence of this calculation from the transport properties point of view is that the HOMO's of the two molecules are shifted upwards by approximately 0.35 eV and there is simultaneously a splitting produced by hybridization of $\sim$0.1 eV. If two molecules produce a splitting $t \sim 0.1$ eV in one energy level, a bandwidth of $\sim 4t = 0.4$ eV is readily expected in the limit of infinite molecules in a column. This value is in excellent agreement with experimental findings for HATn [8].

An additional interesting insight can also be gained from the calculation by evaluating the energy cost needed to rotate one molecule with respect to another from the original total energy minimum. The latter is $\sim$120 meV for two HAT1 molecules separated by 4 Å and one of them rotated by 60° from its original orientation in Fig. 6. This energy plays the role of the exchange energy in a model of classical spins. If we consider a linear chain of classical spins with interaction J connecting the angular variable θ_i at each site with its neighbors θ_{i+1} and θ_{i-1}, we know that in the limit of an infinite chain we need a much lower energy than J to produce excitations. Taking into account that $k_B T \sim 28$ meV at room temperature, we expect a column of molecules in one of the discotic liquid crystalline mesophases to be considerably affected by both static and dynamic disorder. The *defects* in such a chain are either localized (a single molecule rotated with respect to its closest neighbors) or extended (a twist wave), the latter being of lower energy than the former. A more realistic picture should include the effect of the side columns, which are certainly coupled. The energy needed to rotate one molecule with respect to another is certainly related to the transition temperature from the D_{ho} to the H phase, in the same manner that the critical temperature T_c is related to J in a spin model of magnetism. Its exact value cannot be obtained, however, from the interaction between two molecules.

By studying the interaction of two HAT1 molecules we learned the following: (i) the molecules minimize their total energy in the interaction by rotating along the columnar axis;

TABLE V. Calculated basic electronic properties with the AM1 Hamiltonian for $AlCl_3$ and $AlCl_3^-$. The optimized geometry of the neutral molecule corresponds to a planar structure with D_{3h} symmetry and a distance of 1.874 Å between Al and Cl. There are small structural changes upon doping in $AlCl_3^-$; the Al-Cl distance is changed to 2.25 Å and there is a small tendency to abandon the planar structure but preserving the D_{3h} symmetry. See text for further details.

AM1 Hamiltonian	$AlCl_3$	$AlCl_3^-$
Total energy (eV)	−1176.318	−1177.954
Electronic energy (eV)	−2207.660	−2082.485
Core-core repulsion (eV)	1031.342	904.531
Ionization potential (eV)	12.494	3.513
Heat of formation (kcal)	−140.304	−178.026

(ii) there is a crossover in the total energy as a function of distance around ~ 4 Å, which sets a minimum value for the intracolumnar distance, this value represents some sort of an effective hard-core potential for the molecule in the direction perpendicular to the phenyl rings; (iii) the highest occupied molecular levels formed by the delocalized electrons in the triphenylene cores hybridize with an effective hopping that would produce a bandwidth of the order of ~0.4 eV in the columnar mesophases. The band is, however, full and electrons have to be removed to transform it into a hole band for conduction. This is where the doping with aluminum trichloride comes into play and is the subject of the next section; and, finally, (iv) the molecules can rotate inside the columns with a moderate energy cost suggesting a strong influence of static and dynamic disorder in the electronic structure of the chain. A molecule that is misplaced from its position of minimum energy in the column reduces the effective hopping with its neighbors by half according to our calculations. From the point of view of band theory, this represents a perturbing potential with a strength comparable to the bandwidth and can therefore induce localization according to Anderson's criterion. A picture right in the boundary between bandlike and hoppinglike conduction among localized states emerges for these compounds [14,38,39].

D. Hole doping with $AlCl_3$

In this section, we briefly treat the doping process with the electron acceptor $AlCl_3$. We give a tentative picture and avoid the fine details of the fairly entangled subject of reaction dynamics between complex molecules in a liquid crystal. To this end, we attack the problem from the total energy point of view and give some results from AM1 for the molecules involved. Firstly, we give in Table V the calculated electronic properties of $AlCl_3$ obtained with AM1. By the same token, we give the calculated change in total energy in $AlCl_3^-$ produced by adding one electron to the molecule. The structural parameters of the molecule are given in the caption. Note that $AlCl_3$ *gains* approximately ~1.64 eV when it accepts an additional electron. This additional electron has to be extracted from HAT*n* to produce hole doping in the HOMO band as explained in the previous section. It is worth noting that the total energies of the molecules with or without one electron cannot be obtained from the energy diagrams shown in Fig. 5. The Hartree-Fock self-consistent field with AM1 has to be recalculated with one electron either added or missing from the molecule. Strictly speaking, the geometries have to be reoptimized equally because small changes to adapt to the new electronic clouds occur; we have done so in $AlCl_3$ but we ignore the structural reoptimization in the doped discotics since the computation time becomes unmanageable.

As before, we use a HAT1 molecule as representative of the HAT*n* family in the calculation. In what follows we give a brief description of the principal results obtained by the AM1 Hamiltonian for HAT1 and $AlCl_3$: (i) a single HAT1 molecule does not react directly with $AlCl_3$; this is a fairly well known experimental fact; (ii) the total energy of a single HAT1 molecule increases by ~6.54 eV with respect the value listed in Table III when an electron is extracted from the molecule. Note that this value is lower than the ionization potential, accounting for the change in the electronic self-consistent field; (iv) the hole (or missing electron) is localized in the central phenyl rings and the same calculation performed on a HAT4 molecule renders a ground state energy of −8108.48 eV, i.e., an increase of ~6.50 eV with respect to the value given in Table III. The latter is another manifestation of the common features of the ground states of HAT1 and HAT4. These changes in total energy explain, on the other hand, the reason for a HAT*n* molecule not to react directly with $AlCl_3$. In order for a reaction to take place spontaneously, energy must be gained in the process. Experimentally, it is well known that $AlCl_3$ does not react directly with, for example, HAT6 at room temperature [1]. The doping process is carried out by heating a mixture of HAT6 and $AlCl_3$ to 373 K where the discotic liquid crystal is isotropic. In Ref. [5] it was proposed that the reaction involved in the case of HAT6 is

$$3\mathrm{HAT6}+4\mathrm{AlCl_3}\rightarrow 3(\mathrm{HAT6^+AlCl_4^-})+\mathrm{Al}. \qquad (1)$$

However, it is possible to think of a direct reaction path with the columnar phases once the electrons start to be shared among several molecules. It is quite clear that the increase in temperature did not cause the reaction since 373 K ~ 32 meV and this is still not enough to compensate the energy differences needed to capture one electron in $AlCl_3$ extracted from HAT*n*. Experimentally, the temperature must be increased above the isotropic to D_{ho} transition temperature to allow the diffusion of the molecules to take place. The latter is far more efficient and homogeneous in the isotropic than in the columnar mesophase. Once the dopant is distributed throughout the liquid crystal and cooled (and casting aside the effect of temperature as a possible reason for the reaction) the electron extraction from HAT*n* has to involve several molecules in the reaction. From the total energy point of view, we note that a single $AlCl_3$ molecule can gain an electron from the HOMO band only if it is shared by a minimum of 5 to 6 HAT*n* molecules. Consequently, this would suggest a maximum mole fraction doping achievable of ~0.16−0.2. The maximum doping found experimentally amounts to a mole fraction around ~0.15. The theoretical estimate is however quite rough and should be taken with the utmost care. The evaluation of the energy potential surface of the two molecules in the neighborhood is also a very time consuming exercise from the computational point of view.

We have, notwithstanding, calculations of the interaction energy in the equatorial plane of the molecule that suggest that $AlCl_3$ is better placed close to the side branches instead of directly above the phenyl rings. This would imply a picture of $AlCl_3$ playing a minor role in the conduction process through the HOMO band itself, except for the number of carriers it contributes.

IV. CONCLUSIONS

We presented a general overview of the electronic structure of the family of molecules HAT*n*. The specific electronic structures and optimized geometries of two members of the family, HAT1 and HAT4, have been discussed. The interaction process of two HAT1 molecules that ultimately leads to the interesting phenomenon of quasi-one-dimensional conduction also has been discussed. Lastly, the doping process by aluminum thrichloride ($AlCl_3$) has been briefly presented. We hope this work makes a small contribution to a better quantitative understanding of these molecules as well as to a qualitative knowledge of molecules with similar conducting properties. It is important to take into account that the calculations tried to stress the common features of the electronic structures of the different HAT*n* molecules and this implies *per se* a simplification. There is, for example, experimental evidence that transport properties in HAT5 are bandlike but HAT6 has apparently a more dispersive mechanism [8] for conduction. These differences are not yet understood in light of the experimental evidence accumulated so far [8] and will require a more detailed treatment of disorder effects in the columnar mesophases that take into account the effects of chain flexibility, intercolumn interactions, etc. We hope this work stands as a first endeavor in that direction.

ACKNOWLEDGMENTS

Thanks are due to A. Fainstein and to Willy Pregliasco for general support in Bariloche where this work has been performed.

[1] N. Boden, R. J. Bushby, J. Clements, M. V. Jesudason, P. F. Knowles, and G. Williams, Chem. Phys. Lett. **152**, 94 (1988); **154**, 613 (1989).

[2] L. Y. Chiang, J. P. Stokes, C. R. Safinya, and A. N. Bloch, Mol. Cryst. Liq. Cryst. **125**, 279 (1985).

[3] J. van Keulen, T. W. Warmerdam, R. J. M. Nolte, and W. Drenth, Recl. Trav. Chim. Pays-Bas. Recl. Trav. Chim. Pays-Bas. **106**, 534 (1987).

[4] G. B. M. Vaughan, P. A. Heiney, J. P. McCauley, Jr., and A. B. Smith, Phys. Rev. B **46**, 2787 (1992).

[5] N. Boden, R. J. Bushby, and J. Clements, J. Chem. Phys. **98**, 5920 (1993).

[6] For a review on the different mesophases of discotic liquid crystals as well as some optical, mechanical, and structural properties see S. Chandrasekhar and G. S. Raganath, Rep. Prog. Phys. **53**, 57 (1990).

[7] If the interaction were attractive the system would collapse into a polymerlike chain or molecular crystal which is, of course, not the case in a discotic liquid crystal.

[8] N. Boden, R. J. Bushby, J. Clements, B. Movaghar, K. J. Donovan, and T. Kreouzis, Phys. Rev. B **52**, 13 274 (1995).

[9] See also previous related works in H. J. Keller, D. Nöthe, H. Pritzkow, D. Wehe, M. Werner, P. Koch, and D. Schweitzer, Mol. Cryst. Liq. Cryst. **62**, 181 (1980); C. Krohnke, V. Enkelmann, and G. Wegner, Angew. Chem. Int. Ed. Engl. **19**, 912 (1980); J. van Keulen, T. W. Warmerdam, R. J. M. Nolte, and W. Drenth, Recl. Trav. Chim. Pays-Bas. **106**, 534 (1987); D. Schweitzer, Mol. Cryst. Liq. Cryst. **120**, 213 (1985).

[10] N. Boden, R. C. Borner, D. R. Brown, R. J. Bushby, and J. Clements, Liq. Cryst. **11**, 325 (1992).

[11] The conductivity perpendicular to the columns is normally two to three orders of magnitude smaller ($\sigma_\perp \sim 10^{-7}\Omega^{-1}\,\mathrm{cm}^{-1}$) in the doped samples. Both $\sigma_\parallel$ and $\sigma_\perp$ increase above a certain frequency of the order of a few kHz [10].

[12] M. A. Abkowitz, M. J. Rice, and M. Stolka, Philos. Mag. B **61**, 25 (1990); M. Gailberger and H. Bässler, Phys. Rev. B **44**, 8643 (1991).

[13] D. Adam, F. Closs, T. Frey, D. Funhoff, D. Haarer, H. Ringsdorf, P. Schuhmacher, and K. Siemensmeyer, Phys. Rev. Lett. **70**, 457 (1993).

[14] D. Adam, W. Römhildt, and D. Haarer, Jpn. J. Appl. Phys. 1 **135**, 1826 (1996).

[15] D. Adam, P. Schuhmacher, J. Simmerer, L. Häussling, K. Siemensmeyer, K. H. Etzbach, H. Ringsdorf, and D. Haarer, Nature (London) **371**, 141 (1994).

[16] K. Otha, A. Takagi, H. Muroki, I. Yamamoto, and K. Matsuzaki, Mol. Cryst. Liq. Cryst. **147**, 15 (1987).

[17] M. J. S. Dewar, E. G. Zoebisch, E. F. Healy, and J. J. P. Stewart, J. Am. Chem. Soc. **107**, 3902 (1985).

[18] M. J. S. Dewar and W. Thiel, J. Am. Chem. Soc. **99**, 4899 (1977).

[19] For calculations on polymers with the MNDO or previous methods see M. J. S. Dewar, G. P. Ford, and H. S. Rzepa, Chem. Phys. Lett. **50**, 262 (1977); M. J. S. Dewar, S. H. Suck, and P. K. Weiner, *ibid.* **29**, 220 (1974); M. J. S. Dewar, Y. Yamaguchi, and S. H. Suck, *ibid.* **50**, 259 (1977).

[20] M. J. S. Dewar, S. H. Suck, P. K. Weiner, and J. G. Bergman, Jr., Chem. Phys. Lett. **38**, 226 (1976); M. J. S. Dewar and J. J. P. Stewart, *ibid.* **111**, 416 (1984); M. J. S. Dewar, Y. Yamaguchi, and S. H. Suck, *ibid.* **59**, 541 (1978).

[21] The underlying theory of the semiempirical molecular orbitals theories like AM1 and MNDO can be found in any of the classic books in the field like R. G. Parr, *The Quantum Theory of Molecular Electronic Structure* (W. A. Benjamin, New York, 1963); M. J. S. Dewar, *The Molecular Orbital Theory of Organic Chemistry* (McGraw-Hill, New York, 1969); J. N. Murrell and A. J. Harget, *Semiempirical Self-Consistent-Field Molecular Orbital Theory of Molecules* (Wiley, New York, 1972); T. Clark, *A Handbook of Computational Chemistry* (Wiley, New York, 1985).

[22] M. J. S. Dewar, J. Mol. Struct. **100**, 41 (1983).

[23] J. J. P. Stewart, in *Reviews in Computational Chemistry* , edited by K. B. Lipkowitz and D. B. Boyd (VCH, New York, 1990), Vol. 1, p. 45.

[24] W. Thiel, in *Advances in Chemical Physics*, edited by I. Prigogine and Stuart A. Rice (Wiley, New York, 1996), p. 703.

[25] Obtainable from *The Quantum Chemistry Program Exchange* (QCPE), Dept. of Chemistry, Indiana University, Bloomington, Indiana 47405.

[26] J. H. Callomon, T. M. Mills, and I. M. Mills, Philos. Trans. R. Soc. London, Ser. A **259**, 499 (1966); D. M. Burland and G. W. Robinson, J. Chem. Phys. **51**, 4548 (1969); C. S. Parmenter, K. Tang, and W. R. Ware, Chem. Phys. **17**, 359 (1976); J. R. Lombardi, T. W. Hänsch, R. Wallenstein, and D. M. Friedrich, J. Chem. Phys. **65**, 2357 (1976); E. Riedle, H. J. Neusser, and E. W. Schlag, *ibid.* **75**, 4231 (1981).

[27] Y. Endo, S. Saito, and E. Hirota, J. Chem. Phys. **81**, 122 (1984); G. Inone, H. Akimoto, and M. Okuda, *ibid.* **72**, 1769 (1980); P. G. Carrick, S. D. Brossard, and P. C. Engelking, *ibid.* **83**, 1995 (1985).

[28] D. Bloor, Chem. Phys. Lett. **40**, 323 (1976).

[29] V. P. Spiridonov, A. G. Gershikov, E. Z. Zasorin, N. I. Popenko, A. A. Ivanov, and L. I. Ermolayeva, High. Temp. Sci. **14**, 285 (1981).

[30] J. J. P. Stewart, MOPAC [25] manual, sixth edition (1990).

[31] The differences between the optimized geometries predicted by the MNDO and AM1 Hamiltonians are minor. The relative orientation of the three hydrogens in the CH_3 endings with respect to the plane defined by the aromatic rings tends to be different in the AM1 and MNDO calculations. This is the main difference in the optimized geometries obtained by the two methods and is of no consequence in the overall electronic structure. All the other angles and all bond distances are within a few percent when compared in the two calculations.

[32] The optical properties of any substance in the transparency region and, in particular, the anisotropies of the dielectric tensor and the dispersion depend mainly on the first optically allowed transitions. See *Optics and Nonlinear Optics of Liquid Crystals* (Ref. [33]), p. 75 and M. Cardona in *Atomic Structure and Properties of Solids*, edited by E. Burstein (Academic, New York, 1972), p. 513.

[33] I. C. Khoo and S. T. Wu, *Optics and Nonlinear Optics of Liquid Crystals* (World Scientific, London, 1993), p. 7.

[34] As is well known in molecular physics the excited states must include the configuration interaction which is produced by the change in the self-consistent Hartree-Fock field obtained by removing an electron from the highest occupied to the lowest unoccupied molecular orbitals. The Hamiltonian is rediagonalized in a truncated basis of states usually chosen to include mono- and di-excitations. The resulting eigenvalues are the energies of the excited states and can give the exact position of the absorption edge. See *Modern Molecular Photochemistry* (Ref. [35]) for further details.

[35] N. J. Turro, *Modern Molecular Photochemistry* (University Science Books, New York, 1991).

[36] E. Fontes, P. A. Heiney, and W. H. de Jeu, Phys. Rev. Lett. **61**, 1202 (1988).

[37] S. H. J. Idziak, P. A. Heiney, J. P. McCauley Jr., P. Carroll, and A. B. Smith, Mol. Cryst. Liq. Cryst. **237**, 271 (1993).

[38] V. M. Agranovich and A. A. Zakhidov, Chem. Phys. Lett. **50**, 278 (1977).

[39] S. Alexander, J. Bernasconi, W. R. Schneider, and R. Orbach, Rev. Mod. Phys. **53**, 175 (1981).